Materials Research Proceedings 41 (2024) 290-299 https://doi.org/10.21741/9781644903131-33

Microstructure mastering and fatigue behavior of duplex stainless steel obtained with laser powder bed fusion

PIRAS Maxime[1,a*], HOR Anis[1,b] and CHARKALUK Eric[2,c]

[1]Institut Clément Ader (ICA), Université de Toulouse, CNRS, ISAE-SUPAERO, UPS, INSA, Mines-Albi, 3 rue Caroline Aigle, 31400 Toulouse, France

[2]Laboratoire de Mécanique des Solides (LMS), CNRS, UMR 7649, Ecole Polytechnique, Palaiseau Cedex 91128, France

[a]maxime.piras@isae-supaero.fr, [b]anis.hor@isae-supaero.fr, [c] eric.charkaluk@polytechnique.edu

Keywords: LPBF, Microstructure, Fatigue behavior, Duplex SAF 2507

Abstract. Microstructure and mechanical behavior of duplex stainless steels (DSS) are well known when elaborated with conventional processes. Nowadays, many studies aimed to characterize this material for additive manufacturing (AM) processes like laser powder bed fusion (LPBF) [1], [2]. The as-built LPBF microstructure of this alloy is totally ferritic [1]. Heat treatments are therefore necessary to recover the duplex microstructure. These heat treatments need to be optimized. The effects of annealing heat treatments on the microstructure and mechanical behavior of DSS are now known [2], but the consequences on its fatigue strength need to be explored. In this study, firstly, the duplex microstructure will be controlled by heat treatments to obtain austenitic phase with different grain morphology. Then, the influence of microstructure on tensile high cycle fatigue behavior will be investigated. As a result, a microstructure with coarser austenite grains has no effect on fatigue behavior compared to the fully ferritic As-built material whereas the finer microstructure allows an improvement. Even if there is austenite phase improving the material ductility, fatigue damage initiation is always due to pore defects.

Introduction

Since the first apparition of (DSS) in the XXth century, the interests in the properties of this grade of stainless steel leads to its well and further development [3]. Through the years, several grades of DSS were developed increasing their properties such as higher strength, better resistance against intergranular, pitting and crevice corrosion, higher resistance against hydrogen embrittlement, better fatigue and fatigue-corrosion behaviors [4], [5]. Current grades are DSS, super DSS (SDSS) and hyper DSS according to Pitting Resistance Equivalent (PRE) value [4]–[6]. Thanks to these high properties, DSS are used in several industrial fields like oil and gas, paper industry, desalination plant, chemical transport, storage tank [3], [5].

Secondly, AM technologies allow manufacturing parts with more freedom and more complexity. The layer-by-layer processes unlocks new possibilities of design and production. These technologies are available for different domains and materials and is an important subject of researches [7]–[9]. The additively manufactured DSS investigated in the literature are SAF 2205 and SAF 2507. The difficulty to obtain an as-built dual phase microstructure by LPBF process is highlighted by several authors [1], [10], [11]. Even if different energy densities are used, varying process parameters such as laser power, scan speed or layer thickness, a fully ferritic as-built structure is always obtained with this process [12], [13]. This result is mainly explained by the higher cooling rate of the LPBF process leaving no time for nucleation of austenite phase [7]. Thanks to heat treatments (HT), it is possible to obtain austenite phase with an austenite-ferrite phases ratio near to 50-50 and thus improve ductility [2], [10], [11].

In this study, a high-density material is obtained using a parametric optimization. Different HT will be realized to control the microstructure and obtain coarser grain than observed in literature. Then the influence of these microstructures on the high cycle fatigue (HCF) will be studied.

Material and methods

Powder:

The material used in this study is a SDSS SAF 2507 (UNS S32750, X2CrNiMoN25-7-4) commercialized by Sandvik Osprey LTD. The powder is gas-atomized under nitrogen atmosphere with a granulometry of 20 - 45 µm. Figure 1a shows particle size distribution of the powder obtained using a laser diffraction analyzer. Figure 1b reveals that there are some satellites on the powder. The composition of the powder is given in Table 1.

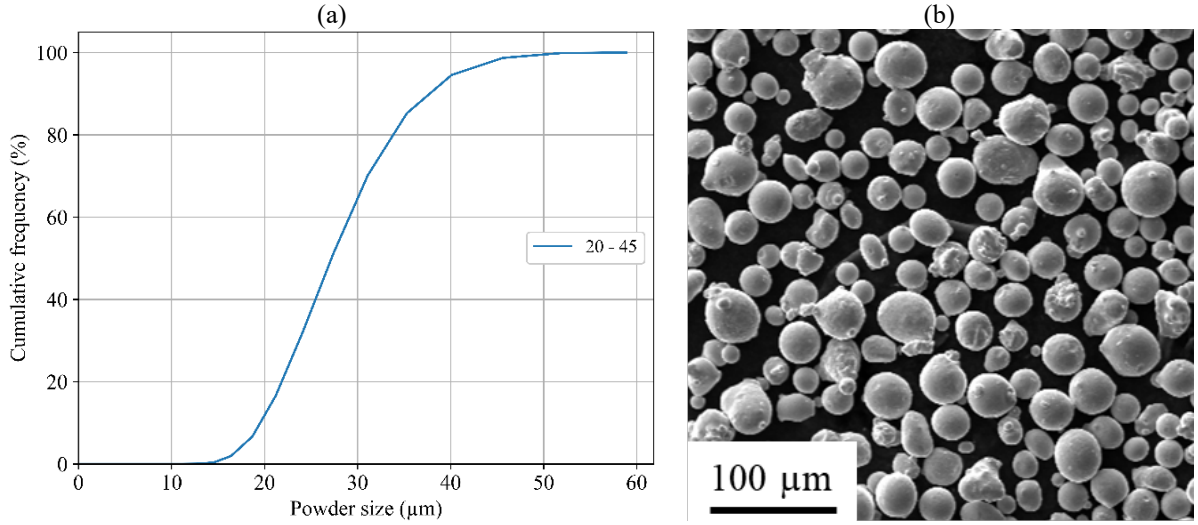

Figure 1: (a) The cumulative particle size distribution obtained by laser granulometry and (b) SEM image of the SAF2507 powder.

Table 1: Chemical composition (wt. %) of the SAF 2507 powder.

Element	Fe	Cr	Ni	Mo	Mn	Si	N	O	Cu	C	Co	Al
wt. %	Bal.	25.0	7.1	3.93	0.8	0.4	0.3	0.06	0.05	0.02	0.1	0.01

Sample manufacturing:

Samples were manufactured using SLM 125HL machine from SLM Solutions. An inert atmosphere under argon was maintained allowing an oxygen level lower than 0.1 %. The substrate was pre-heated at 100 °C. Based on literature [1], [9]–[11], [14], [15], one set of parameters was selected according to its respective volumetric energy density (VED), defined by:

$$\mathrm{VED} = \frac{P}{v \times h \times t} \qquad [J.mm^{-3}] \tag{1}$$

Where, P is the laser power, v the laser scan speed, h the hatch distance and t the layer thickness. The values of the process parameters are illustrated in Table 2. Back-and-forth laser scanning strategy is used without contouring nor chess pattern. The 67° rotation of laser direction between each layer is also applied.

Table 2: Process parameters used for the LPBF process.

VED (J.mm^{-3})	P (W)	v (mm.s^{-1})	h (mm)	t (mm)
115	280	600	0.09	0.045

Heat treatments:
As observed in literature it is mandatory to realize HT to achieve duplex microstructure [1], [10], [11], [16]. To study the effect of HT, temperature ranging from 1100 °C to 1275 °C and holding time ranging from 15 min to 3 h were tested. All the HT are followed by a water quenching to avoid deleterious precipitation (sigma phase).

Characterization methods:
To determine the defect population of the material, X-ray Computed Tomography (CT) scanning was realized with Easytom RX 130 device. A voxel size of $(6.46)^3$ µm^3 is obtained using a tension of 130 V, an intensity of 61 µA and an exposure time of 4 image.s^{-1}. The volume of the gauge length of the fatigue specimen (Figure 2) was analyzed: cylinder with a diameter of 6 mm and a length of 10 mm.

To get detailed information about microstructure and grains, Electron BackScatter Diffraction (EBSD) analysis is realized with FEG JSM 7100F TTLS LS SEM from JEOL and equipped with the CMOS Symmetry S2 EBSD detector from Oxford Instruments. Size map is 804 x 603 µm² ans pixel size is 0.25 x 0.25 µm². The observed sections are parallel to the Building Direction (BD).

Tensile High Cycles Fatigue (HCF) tests are realized with a loading ratio of R = -1 and a frequency of f = 15 Hz. The test run-out is set at 2.10^6 cycles. To determine the HCF limit, the staircase method is used with a step of 20 MPa. The fatigue specimens (Figure 2) are obtained by machining from as-built and heat-treated cylinders with a diameter of 13 mm and a length of 95 mm. After machining, all specimens were grinded and polished with silica paper from P600 to P4000 to avoid influence of surface roughness on fatigue behavior. Finally, Fractography analysis were realized with a Zeiss SEM EVO 10 to determine fracture mechanisms.

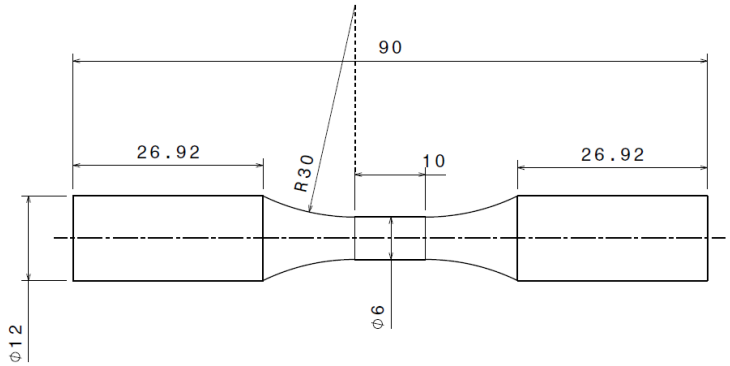

Figure 2: Geometry of fatigue specimen (dimensions in mm).

Results and discussions
Duplex microstructure control:
Firstly, the relative density obtained is higher than 99.93 % for each batch. Samples can be considered as high-density materials. Nevertheless, Figure 3 shows that even with high-density material, there still are defects. Those have a Feret diameter lower than 200 µm and an overall sphericity higher than 0.5. It can be considered as pore defects.

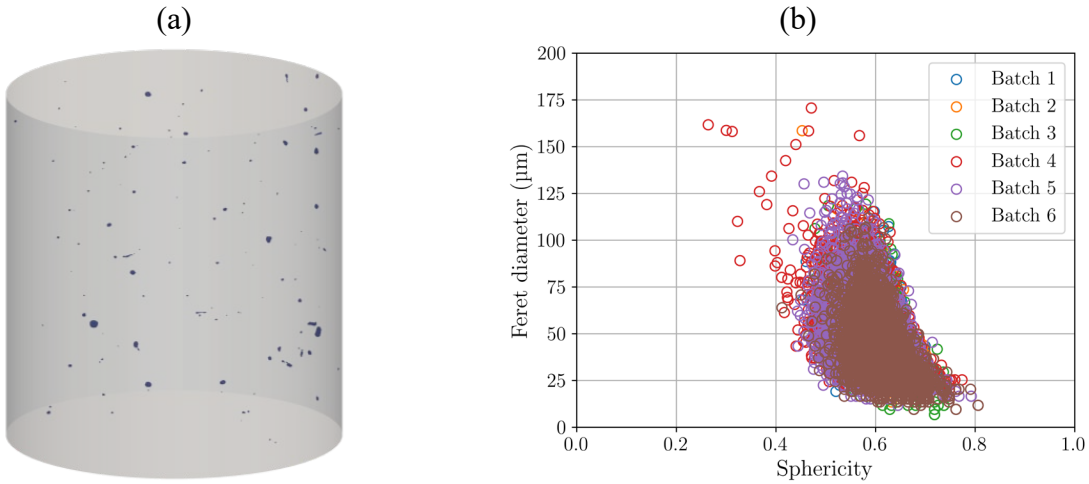

Figure 3: (a) Example of spatial distribution of defects obtained by CT scans of the analyzed volume, and (b) Feret diameter versus sphericity of the defects for each produced batch.

Then, due to the very higher cooling rate characterizing the LPBF process [9], the as-built microstructure is nearly fully-ferritic. It is confirmed on the phase maps in Figure 4a where austenite phase ration is lower than 1 %. HT are therefore necessary to create the austenite phase and thus obtain a duplex (dual phase) microstructure. The <001> preferred orientation is observed in the orientation map illustrated in Figure 4b and confirmed by the Inverse pole figures (IPF) in Figure 4c. It means that most grains [001] are oriented according to BD.

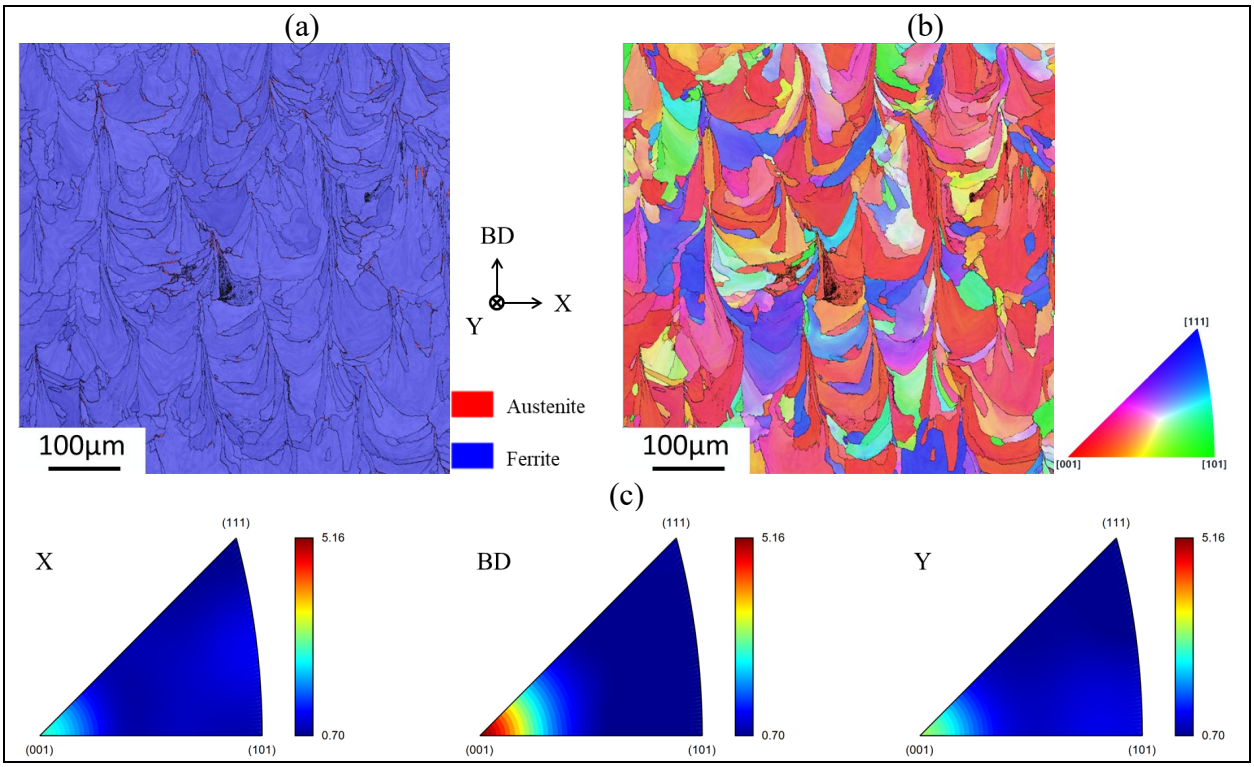

Figure 4: a) Phase map, b) orientation map and c) inverse pole figures of as-built microstructure.

Additionally, as observed in literature, a HT with short holding time is enough to obtain a duplex microstructure with an austenite-ferrite phase fraction ratio near to 50-50 [2], [10], [11] (Figure 5a). Comparing Figure 4a and Figure 5, nucleated austenite grains are both intergranular

and intragranular. With SA_{30} HT, temperature and time are too short to observe grain growth or recrystallization. Only small austenite grains have time to nucleate [10]. Coarser grain morphology is achievable by increasing temperature and holding time (Figure 5b). This grain growth is also accompanied by an imbalance between the two phases: austenite and ferrite. This second HT microstructure (Figure 5b) is composed by 40 % of austenite and 60 % of ferrite (Table 3). To regain the 50-50 balance a second HT is applied. The Double HT (DHT) microstructure is composed by coarser grain with a 50-50 phase ratio as illustrated in Table 3 and Figure 5c.

Finally, austenitic grains as big as those from wrought material (Figure 5d) can be obtained by both DHT and 1275 °C - 3 h HT. Nevertheless, these austenitic grains are not equiaxed.

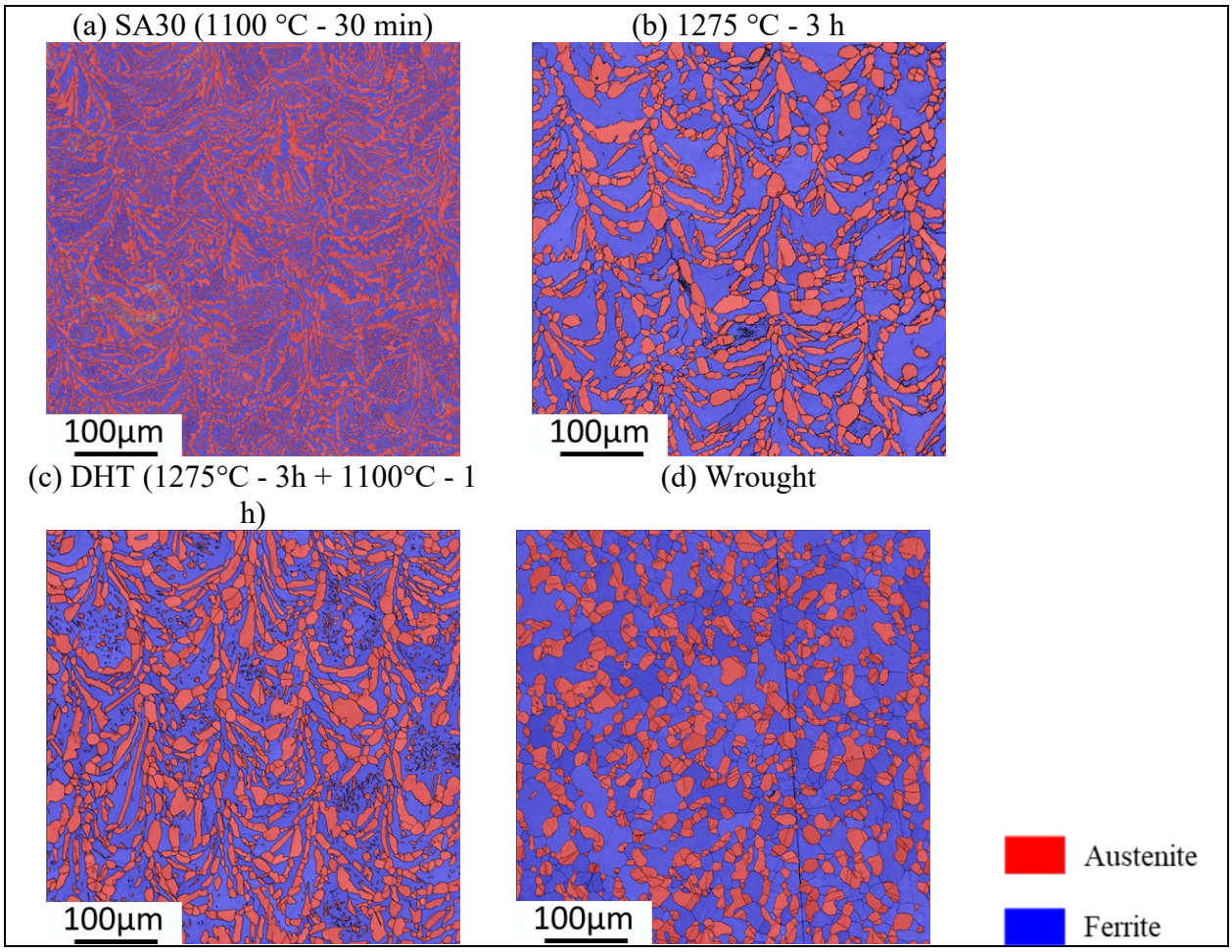

Figure 5: Phase maps of microstructures obtained after different heat treatments and comparison with wrought microstructure (hot rolled and solution heat treated for 1 h at 1050 °C and then water-quenched).

Table 3: Phase fraction obtained after different HT and comparison with wrought microstructure.

HT	Austenite (%)	Ferrite (%)	Sigma (%)
SA_{30}	50.7	49.2	< 0.1
1275 °C - 3 h	39.5	60.4	< 0.1
DHT	50.0	49.9	< 0.1
Wrought	41	59	0

Fatigue behavior:

Discussion about microstructure effect on fatigue behavior is possible because defect population is similar. As observed in Figure 7, at higher stress amplitude (σ_a > 460 MPa), the As-built samples have better fatigue resistance than HT samples. It is in accordance with the higher R_m (Figure 8). While decreasing the stress amplitude, the As-built state becomes less fatigue resistance than SA_{30} HT and then than DHT. It can be explained by the presence of austenite phase for both HT which increases the ductility. A microstructure with coarser grains doesn't improve the fatigue life resistance. Both As-built and DHT specimen show similar fatigue limit (σ_{-1}) even though their fatigue behavior is different (Figure 8a and Figure 8c). An increase of 11 % of fatigue life resistance is obtained for SA_{30} compared to DHT. This is the effect of the smaller austenitic grains obtained for the SA_{30} microstructure (Figure 5a).

The HCF limit of wrought material is close to that obtained for the DHT microstructure. The two microstructure features are similar and the only difference is the presence of LPBF defects in the DHT state. This means that the small LPBF defects obtained in this study (<175 µm as illustrated in Figure 3) have little effect on the fatigue behavior.

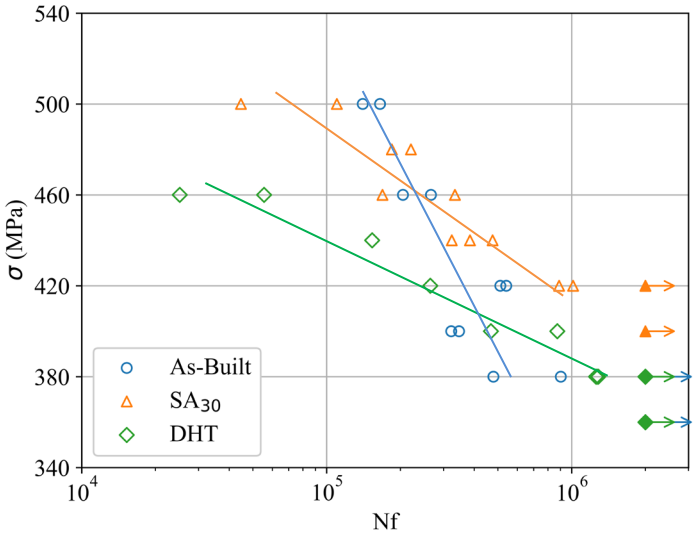

Figure 6: S-N plots obtained for the studied microstructures: as-built, SA30 and DHT.

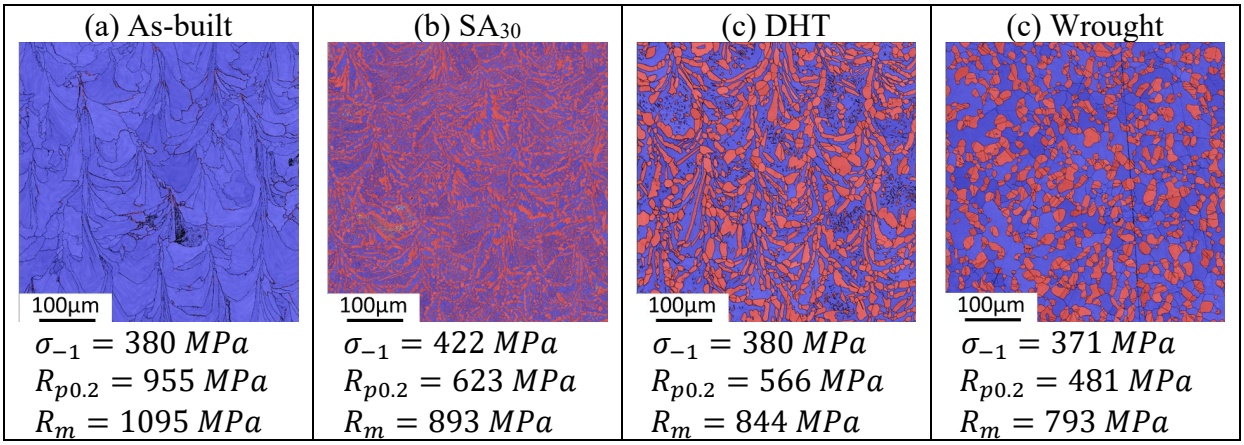

Figure 7: Microstructure, yield stress, ultimate tensile stress and HCF limit of each state: as-built, SA30, DHT and wrought.

However, the crack initiation zone still contains surface pore defect as showed in Figure 9b for all the microstructures. Half of these defects are opening ones. The circularity of these defects is in accordance with the X-ray tomography observations illustrated in Figure 3b. The $\sqrt{area}$ of the pore defects ranges from 30 to 70 µm showing a low dispersion for each sample (Figure 9c). This small defect size confirms that microstructure effect on fatigue behavior can be discussed. The modified Kitagawa-Takachi diagram plotted in Figure 9c shows that there is no defect size effect on fatigue stress amplitude.

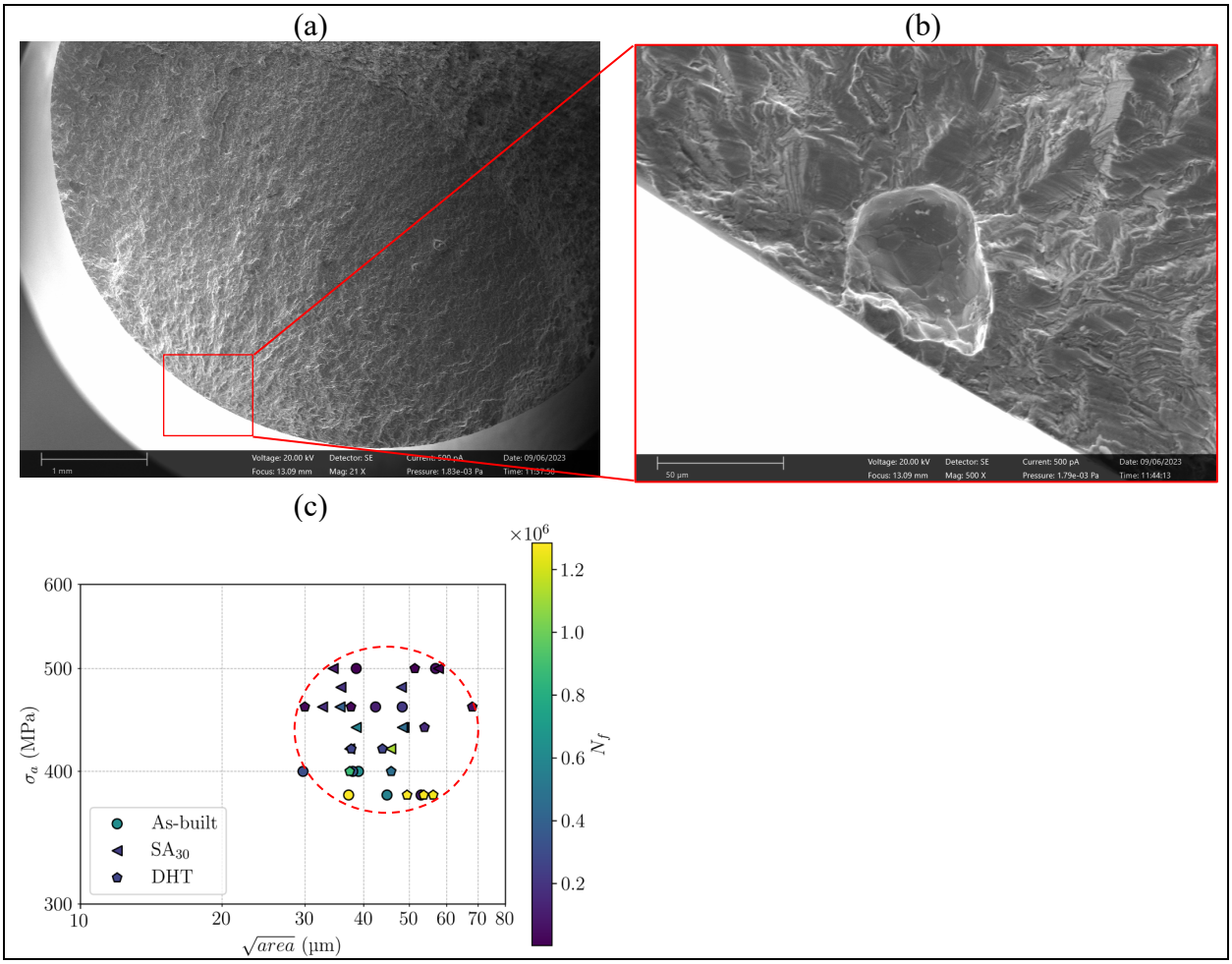

Figure 8: Example of fracture facies of (a) the overall surface, (b) magnification of the initiation zone and (c) the modified Kitagawa-Takachi diagram for the three microstructures: as-built, SA_{30} and DHT.

Conclusion

After successfully building high density LPBF samples, this work aimed at controlling the microstructure of the material and to identify the influence on the fatigue behavior. The main conclusions of this study are:

- LPBF as-built microstructure is ferritic and HT provides a duplex microstructure with different grain morphologies and with austenite-ferrite ratio near to 50-50.
- The coarser duplex microstructure doesn't improve the fatigue life resistance when compared with the As-built material which is fully ferritic.
- In contrary, the smaller microstructure obtained with SA_{30} HT has an impact on the fatigue behavior since an increase of 11 % of the fatigue limit (σ_{-1}) is observed.

References

[1] K. Saeidi, L. Kevetkova, F. Lofaj, and Z. Shen, 'Novel ferritic stainless steel formed by laser melting from duplex stainless steel powder with advanced mechanical properties and high ductility', *Mater. Sci. Eng. A*, vol. 665, pp. 59–65, May 2016. https://doi.org/10.1016/j.msea.2016.04.027

[2] L. Becker *et al.*, 'Influence of annealing time on the microstructure and properties of additively manufactured X2CrNiMoN25-7-4 duplex stainless steel: Experiment and simulation', *Materialia*, p. 101720, Feb. 2023. https://doi.org/10.1016/j.mtla.2023.101720

[3] R. N. Gunn, *Duplex Stainless Steels Microstructure, Properties and Applications*. Woodhead Publishing, 1997. doi: 10.1533/9781845698775.24

[4] M. Knyazeva and M. Pohl, 'Duplex Steels: Part I: Genesis, Formation, Structure', *Metallogr. Microstruct. Anal.*, vol. 2, no. 2, pp. 113–121, Apr. 2013. https://doi.org/10.1007/s13632-013-0066-8

[5] I. Alvarez-Armas and S. Degallaix, *Les aciers inoxydables duplex*. in Traité MIM - Mécanique et Ingénierie des Matériaux Matériaux et métallurgie. Cachan: Hermès science publications, 2012.

[6] G. Chail and P. Kangas, 'Super and hyper duplex stainless steels: structures, properties and applications', *Procedia Struct. Integr.*, vol. 2, pp. 1755–1762, Jan. 2016. https://doi.org/10.1016/j.prostr.2016.06.221

[7] T. DebRoy *et al.*, 'Additive manufacturing of metallic components – Process, structure and properties', *Prog. Mater. Sci.*, vol. 92, pp. 112–224, Mar. 2018. https://doi.org/10.1016/j.pmatsci.2017.10.001

[8] T. Mukherjee, J. S. Zuback, A. De, and T. DebRoy, 'Printability of alloys for additive manufacturing', *Sci. Rep.*, vol. 6, no. 1, Art. no. 1, Jan. 2016. https://doi.org/10.1038/srep19717

[9] K. Davidson and S. Singamneni, 'Selective Laser Melting of Duplex Stainless Steel Powders: An Investigation', *Mater. Manuf. Process.*, vol. 31, p. 150930095558007, Sep. 2015. https://doi.org/10.1080/10426914.2015.1090605

[10] F. Hengsbach *et al.*, 'Duplex stainless steel fabricated by selective laser melting - Microstructural and mechanical properties', *Mater. Des.*, vol. 133, pp. 136–142, Nov. 2017. https://doi.org/10.1016/j.matdes.2017.07.046

[11] S. Papula *et al.*, 'Selective Laser Melting of Duplex Stainless Steel 2205: Effect of Post-Processing Heat Treatment on Microstructure, Mechanical Properties, and Corrosion Resistance', *Materials*, vol. 12, no. 15, Art. no. 15, Jan. 2019. https://doi.org/10.3390/ma12152468

[12] K. P. Davidson and S. B. Singamneni, 'Metallographic evaluation of duplex stainless steel powders processed by selective laser melting', *Rapid Prototyp. J.*, vol. 23, no. 6, pp. 1146–1163, Jan. 2017. https://doi.org/10.1108/RPJ-04-2016-0053

[13] P. Murkute, S. Pasebani, and O. Burkan Isgor, 'Metallurgical and Electrochemical Properties of Super Duplex Stainless Steel Clads on Low Carbon Steel Substrate produced with Laser Powder Bed Fusion', *Sci. Rep.*, vol. 10, no. 1, Art. no. 1, Jun. 2020. https://doi.org/10.1038/s41598-020-67249-2

[14] M. Laleh, A. E. Hughes, W. Xu, P. Cizek, and M. Y. Tan, 'Unanticipated drastic decline in pitting corrosion resistance of additively manufactured 316L stainless steel after high-temperature post-processing', *Corros. Sci.*, vol. 165, p. 108412, Apr. 2020. https://doi.org/10.1016/j.corsci.2019.108412

[15] J. Kunz, A. Boontanom, S. Herzog, P. Suwanpinij, A. Kaletsch, and C. Broeckmann, 'Influence of hot isostatic pressing post-treatment on the microstructure and mechanical behavior of standard and super duplex stainless steel produced by laser powder bed fusion', *Mater. Sci. Eng. A*, vol. 794, p. 139806, Sep. 2020. https://doi.org/10.1016/j.msea.2020.139806

[16] K. Saeidi, S. Alvi, F. Lofaj, V. I. Petkov, and F. Akhtar, 'Advanced Mechanical Strength in Post Heat Treated SLM 2507 at Room and High Temperature Promoted by Hard/Ductile Sigma Precipitates', *Metals*, vol. 9, no. 2, Art. no. 2, Feb. 2019. https://doi.org/10.3390/met9020199